Acta Biomaterialia 73 (2018) 388–399

Contents lists available at ScienceDirect

Acta Biomaterialia

journal homepage: www.elsevier.com/locate/actabiomat

Full length article

A polypeptide based podophyllotoxin conjugate for the treatment of multi drug resistant breast cancer with enhanced efficiency and minimal toxicity

Huicong Zhou [a,b], Shixian Lv [b], Dawei Zhang [b], Mingxiao Deng [c], Xuefei Zhang [a,*], Zhaohui Tang [b,*], Xuesi Chen [b]

[a] Key Laboratory of Environmentally Friendly Chemistry and Applications of Ministry of Education and Key Laboratory of Polymeric Materials & Application Technology of Hunan Province, Xiangtan University, Xiangtan 411105, PR China
[b] Key Laboratory of Polymer Ecomaterials, Changchun Institute of Applied Chemistry, Chinese Academy of Sciences, Changchun 130022, PR China
[c] College of Chemistry, Northeast Normal University, Changchun 130024, PR China

ARTICLE INFO

Article history:
Received 23 December 2017
Received in revised form 3 April 2018
Accepted 5 April 2018
Available online 22 April 2018

Keywords:
P-glycoprotein
Podophyllotoxin
Polypeptide
Conjugate
Drug delivery

ABSTRACT

Podophyllotoxin (PPT) is a chemotherapeutic agent which has shown significant activity against P-glycoprotein (P-gp) mediated multi drug resistant cancer cells. However, because of the poor aqueous solubility and high toxicity, PPT cannot be used in clinical cancer therapy. In order to enhance the efficiency and reduce side effect of PPT, a polypeptide based PPT conjugate PLG-*g*-mPEG-PPT was developed and used for the treatment of multi drug resistant breast cancer. The PLG-*g*-mPEG-PPT was prepared by conjugating PPT to poly(L-glutamic acid)-*g*-methoxy poly(ethylene glycol) (PLG-*g*-mPEG) *via* ester bonds. The PPT conjugates self-assembled into nanoparticles with average sizes about 100 nm in aqueous solution. Western blotting assay showed that the PLG-*g*-mPEG-PPT could effectively inhibit the expression of P-gp in the multiple drug resistant MCF-7/ADR cells. *In vitro* cytotoxicity assay indicated that the resistance index (RI) values of PLG-*g*-mPEG-PPT on different drug-resistant cancer cell lines exhibited 57–270 folds reduction than of traditional microtubule inhibitor chemotherapeutic drug PTX or DTX. Hemolysis assay demonstrated that the conjugation greatly decreased the hemolytic activity of free PPT. Maximum tolerated dose (MTD) of PLG-*g*-mPEG-PPT increased greatly (13.3 folds) as compared to that of free PPT. *In vivo* study showed that the PLG-*g*-mPEG-PPT conjugate remarkably enhanced the antitumor efficacy against MCF-7/ADR xenograft tumors with a tumor suppression rate (TSR) of 82.5%, displayed significantly improved anticancer efficacy as compared to free PPT (TSR = 37.1%) with minimal toxicity when both of the two formulations were used in MTD.

Statement of Significance

The development of multiple drug resistance (MDR) of cancer cells is the main cause of chemotherapy failure. The over-expression of P-glycoprotein (P-gp) has been recognized to be the most important cause of MDR in cancer. Podophyllotoxin (PPT) is a chemotherapeutic agent which has shown strong activity against P-gp mediated multidrug resistant cancer cells by simultaneously inhibiting the over-expression of P-gp and the growth of cancer cells. However, PPT can not be used in clinical cancer treatment due to its poor aqueous solubility and high toxicity. Herein, we developed a polypeptide based PPT conjugate PLG-*g*-mPEG-PPT by conjugating PPT to poly(L-glutamic acid)-*g*-methoxy poly(ethylene glycol). The PLG-*g*-mPEG-PPT shows significantly decreased hemolytic activity, greatly improved maximum tolerated dose and remarkably enhanced antitumor efficacy against MCF-7/ADR xenograft tumors as compared to free PPT.

1. Introduction

Cancer is the leading disease that threatens human health. Chemotherapy is still the basic method of clinical malignant tumor

* Corresponding authors.
E-mail addresses: zxf7515@163.com (X. Zhang), ztang@ciac.ac.cn (Z. Tang).

https://doi.org/10.1016/j.actbio.2018.04.016
1742-7061/

therapy [1–4]. To minimize the side effects and improve the therapeutic efficacy of chemotherapy, nanomedicines based on various biomaterials have been devoted in the past decade [5–9]. Among these biomaterials, synthetic polypeptides are one of the most important and widely studied biomaterials [10–12]. The chemical diversity of the side chains of synthetic polypeptides enables their broad applications in the field of gene delivery, bio-imaging and drug delivery [13]. These polypeptide polymers have shown improved aqueous solubility, enhanced *in vivo* stability, and prolonged blood circulation time, which contributed to better performances of drugs in the biological environment [7,14].

In the cancer chemotherapy, the development of multi drug resistant (MDR) of cancer cells during treatment is the main cause of chemotherapy failure and accounts for as more than nearly 90% death of tumor patients [15–18]. So far, the over-expression of P-glycoprotein (P-gp) has been recognized to be the most important cause of MDR in cancer [19–22]. In order to overcome the MDR of cancer cells, various strategies have been developed which largely depend on the combination of MDR inhibitors and chemotherapeutic drugs [23,24]. However, these combination strategies still face challenges that limit their efficacy in overcoming MDR: (1) the toxicity of inhibitors at effective P-gp inhibiting doses, (2) difficulties of regulation and control of the combination dosage accurately [25,26], (3) complexity of the formulation. Thus, specific chemotherapeutics which can simultaneously inhibit the growth of tumor cells and the over-expression of P-gp will be advantageous to treat the drug resistant tumor cells without complicated design.

Podophyllotoxin (PPT) is a kind of lignan anti-tubulin agent extracted from natural plants. After the successful use of PPT to treat venereal warts in 1942, there has been a growing interest in the application of PPT against tumors [27]. PPT can effectively inhibit the assembly of microtubule of tumor cells, therefore, PPT alone has shown potent antitumor activity [28,29]. Later, Podophyllotoxin was found to exhibit significant activity against P-glycoprotein mediated MDR tumor cell lines [30,31]. However, due to the severe side effect caused by nonspecific cytotoxicity and poor water solubility, PPT has not been well applied in cancer treatment [28]. Recently, several PPT-nanoparticle systems have been developed [32–34], however, to the best of my knowledge, polypeptide-based PPT delivery system has never been reported [35–37].

In order to overcome the limitations of free PPT, we describe here the construction of PPT conjugated polymeric nanomedicine for the treatment of multi drug resistant breast cancer. In this design, PPT was conjugated to poly(L-glutamic acid)-*g*-methoxy poly(ethylene glycol) (PLG-*g*-mPEG) copolymer *via* ester bonds to obtain the polymer-drug conjugate PLG-*g*-mPEG-PPT. The PLG-*g*-mPEG-PPT was synthesized, characterized and evaluated *in vitro* and *in vivo* in detail.

2. Materials and methods

2.1. Materials.

PLG-*g*-mPEG was prepared according to our team's previous work [14]. The PLG-*g*-mPEG has an average of 160 L-glutamic acid repeating units and an average of 8.3 $mPEG_{5k}$ chains. PPT was purchased from Dalian Meilun Biological Technology Co., Ltd., China. *N*,*N*-Dimethylformamide (DMF) was stored over CaH_2 for 3 days and distilled under vacuum prior to use. Diisopropylcarbodiimide (DIC), 4-dimethylaminopyridine (DMAP), fluoresceinamine isomer II (FI), 3-(4,5-dimethyl-thiazol-2-yl)-2,5-diphenyl tetrazolium bromide (MTT) and 4′,6-diamidino-2-phenylindole dihydrochloride (DAPI) were all supplied by Sigma-Aldrich Co., LLC. Benzotriazol-1-yl-oxytripyrrolidino-phosphonium hexafluorophosphate (PyBOP) and trypsin were purchased from Aladdin Industrial Corporation, Shanghai, China. For all the *in vitro* and *in vivo* studies, free drugs were first dissolved in an ethanol/castor oil mixture (1:1, v/v) to 6 mg mL^{-1} and then diluted with culture medium or PBS. All other reagents and solvents were purchased from Sinopharm Chemical Reagent Co., Ltd., China and used as received.

2.2. Cells cultures and animals

MCF-7 cells (Human breast cancer cell line), A549 cells (Human non-small cell lung cancer cell line) were obtained from the Cell Bank of the Chinese Academy of Sciences (Shanghai, China). MCF-7/ADR cells (Human breast cancer drug-resistant cell line) were originated from the Cancer Center of the Second Affiliated Hospital of Zhejiang University School of Medicine. A549/PTX cells (Human non-small cell lung cancer paclitaxel-resistant cell line) were obtained from Shanghai Bogu Biotechnology Co., Ltd., China. MCF-7 and A549 cells were cultured at 37 °C in a 5% CO_2 atmosphere in Dulbecco's modified Eagle's medium (DMEM, Gibco) supplemented with 10% fetal bovine serum (FBS), penicillin (50 Um L^{-1}) and streptomycin (50 Um L^{-1}). MCF-7/ADR and A549/PTX cells were maintained in RPMI medium 1640 (Gibco) supplemented with 10% FBS in a humidified atmosphere containing 5% CO_2 at 37 °C.

Female Balb/C nude mice (6–8 weeks old) were purchased from Beijing Huafukang Biological Technology Co. Ltd. (HFK Bioscience, Beijing). Kunming mice (6–8 weeks old, male) were purchased from Laboratory Animal Center, Jilin University (Changchun, China). All experimental animals received well care and approved by the Animal Care and Use Committee of Jilin University.

2.3. Characterizations

^1H NMR spectra were carried on a Bruker AV 400 NMR spectrometer in chloroform-*d* ($CDCl_3$) or trifluoroacetic acid-*d* (CF_3COOD). Dynamic laser scattering (DLS) measurement was performed as our previous study [38,39]. Unconjugated PPT in the PLG-*g*-mPEG-PPT conjugate was determined using a Waters 1525 Binary HPLC pump with the detector set at 220 nm using acetonitrile and water (4:1, v/v) as a mobile phase. Gel permeation chromatography (GPC) measurement of PLG-*g*-mPEG was conducted on a water GPC system (Waters Ultrahydrogel Linear column, 1515 HPLC pump with 2414 Refractive Index detector) using phosphate buffer (0.2 M, pH 7.4) as eluent (flow rate: 1 mL min^{-1} at 25 °C, and polyethylene glycol as standards). GPC measurement of the PLG-*g*-mPEG-PPT was carried out on a GPC system equipped with a Waters 1515 HPLC pump, a series of linear Tskgel Super columns (AW3000 and AW5000), and a OPTILAB DSP interferometric refractometer. The eluent was DMF containing 0.05 M lithium bromide (LiBr) at a flow rate of 1 mL min^{-1} at 50 °C. Poly (methyl methacrylate) (PMMA) standards with different molecular weights were used to generate the calibration curve. The zeta-potential of PLG-*g*-mPEG-PPT was measured by a Zeta Potential/BI-90Plus Particle Size Analyzer (Brookhaven, USA). Critical micelle concentration (CMC) was measured according to the previous method [40]. Confocal laser scanning microscopy (CLSM) observations were performed on a Carl Zeiss LSM 780 confocal laser microscope. Circular dichroism (CD) spectroscopy was performed on Circular dichroism (Applied Photophysics Ltd., UK.). FT-IR spectra were recorded on a Bio-Rad Win-IR instrument using the potassium bromide method.

2.4. Synthesis of PLG-g-mPEG-PPT.

PLG-g-mPEG-PPT was prepared through the condensation reaction of PLG-g-mPEG and PPT using DIC as condensing agent and DMAP as catalytic agent. In brief, PLG-g-mPEG (2.0 g, 0.032 mmol), PPT (534.6 mg, 1.290 mmol), and DMAP (78.7 mg, 0.645 mmol) were added to a flame-dried flask and dissolved in dry DMF (20 mL), then heated gently and stirred for about 0.5 h until the solution was completely clear. Subsequently, DIC (162.5 mg, 1.290 mmol) in 5 mL DMF was added *via* a syringe under the ice bath. The reaction was maintained in the dark at 25 °C for 24 h. The solution was precipitated with excess amount of cold diethyl ether to remove unreacted PPT and other small molecules. The precipitation was repeated twice before pumping vacuum and PLG-g-mPEG-PPT crude product was obtained. Then the crude product was dissolved in DMF and dialyzed against distilled water for 3 days. The purified product was obtained as a white solid after freeze-drying. ^{1}H NMR of PLG-g-mPEG-PPT was measured using CF_3COOD as a solvent. FT-IR spectra of non salinized PLG-g-mPEG, non salinized PLG-g-mPEG-PPT and the freeze-drying product of sodium salinized PLG-g-mPEG (pH 9.0) and sodium salinized PLG-g-mPEG-PPT (pH 9.0) were also recorded.

2.5. Synthesis of FI-labeled PLG-g-mPEG-PPT.

Briefly, PLG-g-mPEG-PPT (200.0 mg), FI (10.0 mg) and PyBOP (22.5 mg) were dissolved in DMF (5 mL) and the reaction solution was stirred for 24 h at room temperature in the dark. Then the mixture was dialyzed against distilled water. The FI-labeled PLG-g-mPEG-PPT yellow powder was obtained after lyophilization and stored at dark place.

2.6. Determination of DLC and DLE of PLG-g-mPEG-PPT.

Drug loading content (DLC, wt%) and drug loading efficiency (DLE, wt%) of the PLG-g-mPEG-PPT were determined by UV–Vis spectrophotometry at 292 nm. DLC and DLE were calculated according to the following formulas:

$$\mathrm{DLC\,(wt\%)} = (\text{weight of loaded PPT}/\text{weight of conjugates}) \times 100\%$$

$$\mathrm{DLC\,(wt\%)} = (\text{weight of loaded PPT}/\text{weight of feeding PPT}) \times 100\%$$

2.7. In vitro drug release study.

The *in vitro* drug release was investigated in PBS buffer (pH 7.4 and pH 5.0) with or without trypsin (0.40 mg mL^{-1}). Typically, weighted PLG-g-mPEG-PPT powder was dissolved in 10 mL of release medium and placed into a dialysis bag (MWCO 3500 Da). Afterwards, the dialysis bag was transferred into 40 mL of release medium. The release study was performed in a thermotank under gently shaking at 100 rpm at 37 °C. At desired time intervals, 4 mL of release solution was withdrawn and replaced with equal amount of fresh release medium. The PPT release amount was determined by UV–Vis spectrometer at 292 nm.

2.8. Cellular uptake

The cellular uptake behaviors of FI-labeled PLG-g-mPEG-PPT were investigated by CLSM toward MCF-7/ADR cells. Cells were seeded on the coverslips in 6-well plates with a density of 1.0×10^5 cells per well in 2 mL of RMPI 1640 medium and incubated for 24 h, then the cells were treated with FI-labeled PLG-g-mPEG-PPT. The culture media were removed after 1 or 3 h incubation at 37 °C. The cells were washed with fresh PBS and fixed with formaldehyde (4% in PBS) for 10 min at 37 °C. Then the cell nuclei were stained with 0.1% DAPI for 10 min in the dark and washed with PBS three times. The treated cells were visualized with a Carl Zeiss LSM 780 confocal laser microscope.

2.9. In vitro cytotoxicity assays.

The *in vitro* cytotoxicity of free PPT, PTX, DTX and PLG-g-mPEG-PPT were evaluated by MTT assay on four tumor cell lines (MCF-7, MCF-7/ADR; A549, A549/PTX). Cells were seeded in 96-well plates at 6.0×10^3 cells per well in 100 μL DMEM or RMPI 1640 medium for 24 h. Subsequently, the original culture medium was removed, fresh culture medium containing free drug (PPT, PTX or DTX) or PLG-g-mPEG-PPT was added in different concentrations. After other 72 h incubation, cell viability was analyzed using MTT assay with a Bio-Rad 680 microplate reader at a wavelength of 490 nm. The relative cell viability was determined by comparing the absorbance at 490 nm with control wells containing only cell culture medium. Data are presented as mean ± STD (n = 3).

2.10. Apoptotic activity

The apoptotic activities of free PPT and PLG-g-mPEG-PPT on MCF-7/ADR cells were determined by fluorescent-activated cell sorting (FACS) using propidium iodide (PI) and annexin V staining. Briefly, MCF-7/ADR cells were seeded in 6-well plates at 3.0×10^5 cells per well and incubated for 24 h, and then treated with free PPT or PLG-g-mPEG-PPT (10 or 20 μM on the PPT basis) for 48 h. The cells were treated with an Annexin V-FITC apoptosis detection kit (KeyGEN Biotech, China) following the manufacturer's instruction. The apoptotic activities of free PPT and PLG-g-mPEG-PPT were performed using flow cytometry in the same manner.

2.11. Western blot analysis

MCF-7/ADR cells were exposed to various concentrations of free PPT and PLG-g-mPEG-PPT for 48 h. Untreated MCF-7 and MCF-7/ADR cells were used as control groups. Then, all the cells were collected and lysed to extract the whole protein. The lysate was cleared by centrifugation, quantified, and boiled at 100 °C for 10 min in SDS loading buffer. Then, the cell extracts were equally loaded onto 8% SDS–PAGE and electrophoretically transferred to PVDF membrane (Bio-Rad, New Orleans, Louisiana, USA). The membrane was blocked with Tris-buffered saline plus 0.1% Tween 20 plus 5.0% skim milk (BSA). Then PVDF membrane was incubated overnight with primary antibody against Mdr-1 (Santa Cruz) at 4 °C. The membrane was then washed with TBST and incubated for 1 h with a secondary antibody before being visualized. Image J was used to analysis the gray-scale values of the straps.

2.12. Hemolysis assay

Hemolytic activities of free PPT and PLG-g-mPEG-PPT were evaluated according to the previous protocol [41]. In brief, fresh rabbit blood obtained from the Experimental Animal Center of Jilin University was diluted by physiological saline and EDTA was added as anticoagulant. After centrifugation, red blood cells (RBCs) were obtained. After carefully washing and diluting, 2% RBC suspension was prepared. Then, free PPT or PLG-g-mPEG-PPT micelle solution at systematically varied concentrations were added and mixed by vortex and incubated at 37 °C for 2 h. PBS and double distilled water were used as negative and positive controls, respectively. After that, RBCs were centrifuged at 3000 rpm for 10 min and 100 μL of supernatant of each sample was transferred to a 96-well plate. Free hemoglobin in the supernatant was measured with

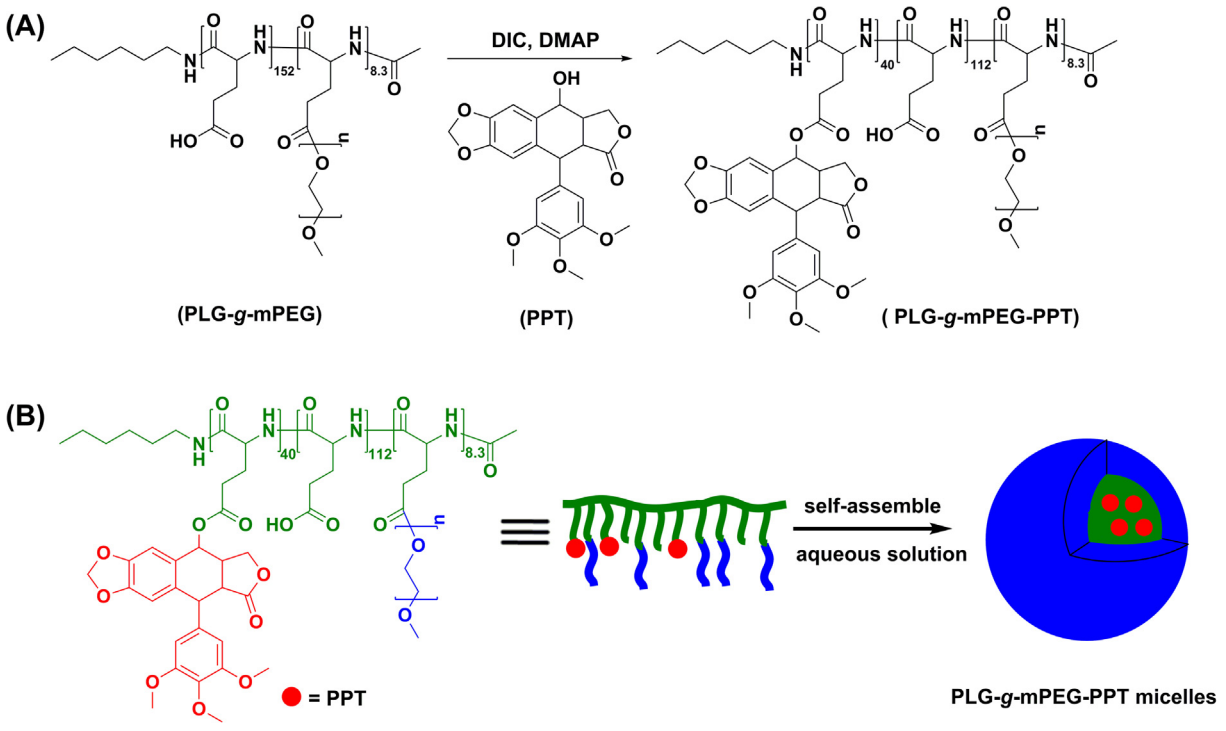

Scheme 1. (A) Preparation of PLG-*g*-mPEG-PPT and (B) self-assemble behavior of PLG-*g*-mPEG-PPT micelles.

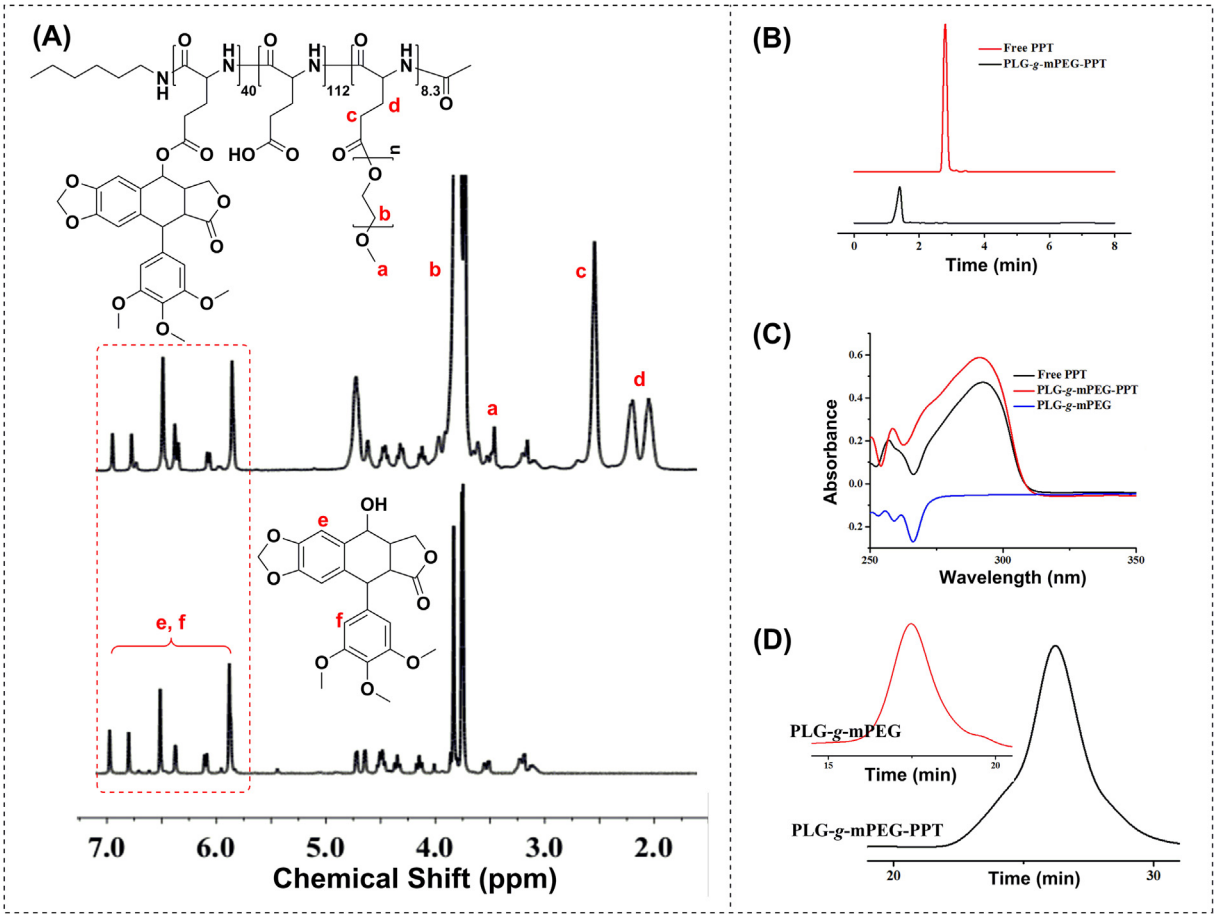

Fig. 1. (A) ^{1}H NMR spectrums of PPT in $CDCl_3$ and PLG-g-mPEG-PPT in CF_3COOD, (B) HPLC curves of free PPT and PLG-g-mPEG-PPT (acetonitrile and water (4:1, v/v) at 220 nm), (C) UV spectrograms of free PPT, PLG-g-mPEG and PLG-g-mPEG-PPT in DMF. (D) GPC curves of PLG-g-mPEG and PLG-g-mPEG-PPT.

a Bio-Rad 680 microplate reader at 540 nm. The hemolysis ratio (HR) of RBCs was calculated using the following formula:

Hemolysis (%) = ($A_{sample} - A_{negative\ control}$)/($A_{positive\ control} - A_{negative\ control}$) × 100%, where A_{sample}, $A_{negative\ control}$, and $A_{positive\ control}$ were denoted as the absorbencies of samples, negative and positive controls, respectively. All hemolysis experiments were carried out in triplicates.

2.13. Maximum tolerated dose (MTD)

Kunming mice were divided into 10 groups (n = 10) and administered intravenously with the free PPT (5, 10, 15, 20, 30 mg kg^{-1}) or PLG-*g*-mPEG-PPT (20, 50, 100, 150, 200, 250, 300 mg kg^{-1} in PPT equivalent). Changes in body weight and survival of mice were measured daily for 2 weeks. The MTD was identified as the maximum dose of a drug that does not induce animal death or >20% body weight loss or other remarkable changes in the general appearance within the entire period of the experiments.

2.14. In vivo anti-tumor efficacy study

MDR human breast tumor xenograft model was established by subcutaneous inoculation of 1.0 × 10^7 MCF-7/ADR cells in 100 μL serum-free RPMI 1640 media into the hind flank of each mouse. When the tumor volume reached about 50–60 mm^3, the mice were divided into 3 groups (n = 4) and then treated with PBS, free PPT (15 mg kg^{-1}), PLG-*g*-mPEG-PPT (200 mg kg^{-1} in PPT equivalent) by tail intravenous injection only one time at day 0. Tumor size and body weight were measured every two days to evaluate the antitumor activity and systemic toxicity. Tumor volume was measured using a Vernier caliper. Tumor volume (V) = a × b^2/2, where a is the length and b is the width of each tumor. Similarly, tumor suppression rate (TSR) was calculated according to the previous calculation method [42]. TSR (%) = [($V_c - V_x$)/V_c] × 100%, where c represents the control group and x represents the treatment group.

2.15. Statistical analysis

Data are expressed as the mean ± STD. Statistical significance was determined using the Student's t-test. $p < 0.05$ was considered statistically significant, and $p < 0.01$ was considered highly significant.

3. Results and discussion

3.1. Synthesis and characterization of PLG-g-mPEG-PPT conjugate

As shown in Scheme 1A, PLG-*g*-mPEG-PPT was simply synthesized by condensation of the hydroxyl group of PPT with the carboxyl groups of PLG-*g*-mPEG. Selection PLG-*g*-mPEG as the vehicle material was because of its excellent biocompatibility, good biodegradability and long blood circulation time [42–46]. The structures of PPT and PLG-*g*-mPEG-PPT were confirmed by ^{1}H NMR in Fig. 1A. The signals at δ 5.89–7.07 ppm were assigned to the protons of phenyl groups of PPT. The appearance of signals of phenyl groups of PPT in the ^{1}H NMR spectrum of PLG-*g*-mPEG-PPT suggested the existence of PPT in the obtained PLG-*g*-mPEG-PPT. HPLC curves of PPT and PLG-*g*-mPEG-PPT were shown in Fig. 1B. The peak of PPT at 2.96 min disappeared in the spectrum of the PLG-*g*-mPEG-PPT, indicating the absence of free PPT in the conjugate. The UV spectra of free PPT, PLG-*g*-mPEG and PLG-*g*-mPEG-PPT were shown in Fig. 1C. PLG-*g*-mPEG had no UV absorp-

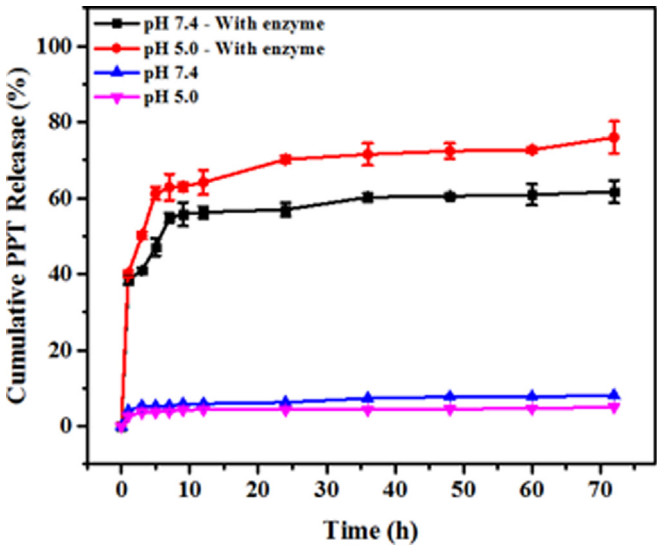

Fig. 3. PPT release profiles of PLG-g-mPEG-PPT in PBS or PBS with enzyme (trypsin at 0.4 mg/mL) at pH 7.4 or 5.0 at 37 °C. Each point was an average of three measurements.

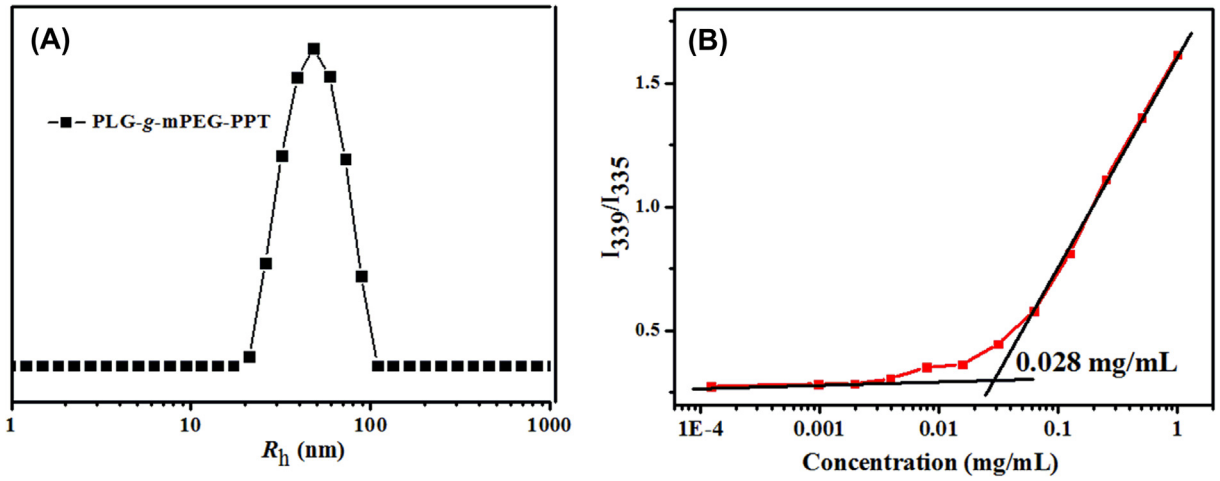

Fig. 2. (A) Hydrodynamic radius, and (B) critical micelle concentration (CMC) of PLG-*g*-mPEG-PPT.

tion in the range of 275–400 nm, both free PPT and PLG-*g*-mPEG-PPT presented the maximum absorption at 292 nm. GPC analyses (Fig. 1D) revealed that the PLG-*g*-mPEG and PLG-*g*-mPEG-PPT had a narrow, unimodal molecular weight distribution (PDI = 1.17 and 1.37, respectively). The FT-IR of non salinized PLG-*g*-mPEG, non salinized PLG-*g*-mPEG-PPT and the freeze-drying product of sodium salinized PLG-*g*-mPEG (pH 9.0) and sodium salinized PLG-*g*-mPEG-PPT (pH 9.0) were shown in Fig. S2. The peaks at 1735 cm^{-1} ($\upsilon_{C(O)-O}$) are attributed to the carboxyl acid groups (–COOH) of poly(*L*-glutamic acid) and carboxylic

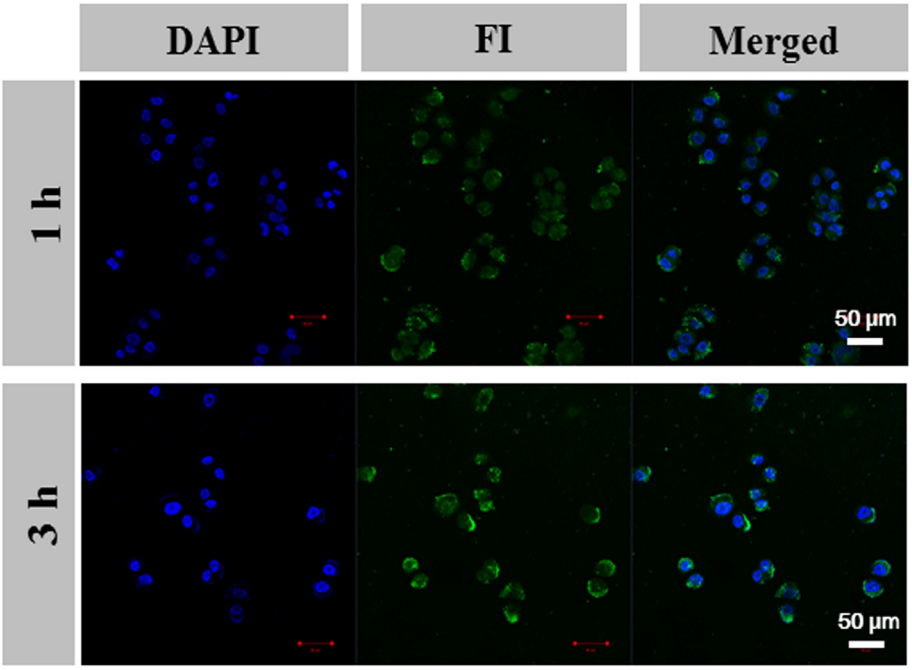

Fig. 4. Confocal laser scanning microscopy observation of MCF-7/ADR cells after incubation with FI-labeled PLG-*g*-mPEG-PPT for 1 and 3 h at 37 °C.

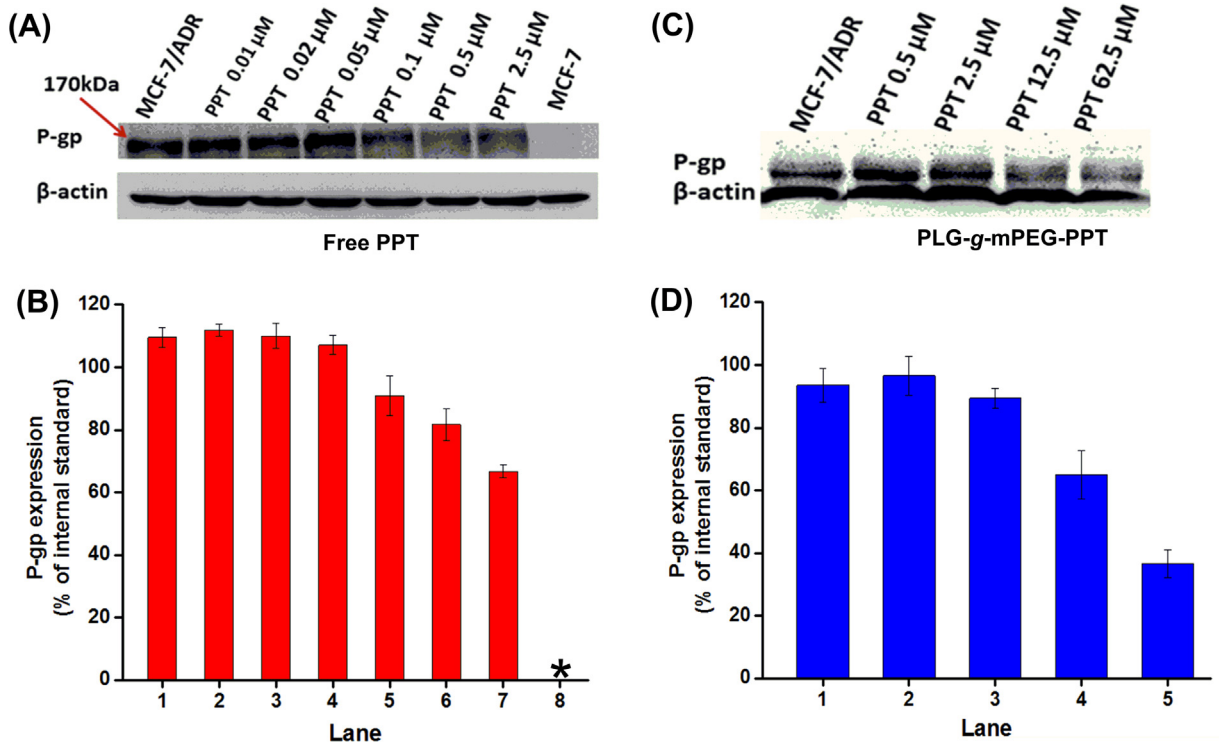

Fig. 5. Effect of P-gp expression in MCF-7/ADR and MCF-7 cells evaluated by western blotting using β-actin as an internal control. (A) Free PPT; (B) Lane 1 represents the untreated MCF-7/ADR control group. Lanes 2–7 represent 0.01, 0.02, 0.05, 0.1, 0.5 and 2.5 μM PPT, respectively. Lane 8 represents the untreated MCF-7 control group. (C) PLG-*g*-mPEG-PPT (PPT equivalent) and (D) Lane 1 represents the untreated MCF-7/ADR control group. Lanes 2–5 represent 0.5, 2.5, 12.5, 62.5 μM PLG-*g*-mPEG-PPT (PPT equivalent), respectively. (n = 3).

ester of PLG-*g*-mPEG-PPT [47]. For non salinized PLG-*g*-mPEG and PLG-*g*-mPEG-PPT, the characteristic peaks (–COOH) at 1735 cm^{-1} were strong. After sodium salinization of the carboxyl groups, this peak disappeared for the PLG-*g*-mPEG because the carboxyl acid groups (–COOH) had changed to carboxylate ions groups ($–COO^-$). In contrast, because of the formation of PLG-PPT ester linkages in the PLG-*g*-mPEG-PPT, the peak at 1735 cm^{-1} still existed for the sodium salinized PLG-*g*-mPEG-PPT. These further confirmed the existence of PPT moiety in the obtained PLG-*g*-mPEG-PPT. Standard curve of free PPT was obtained and DLC of the PLG-*g*-mPEG-PPT was determined by UV–Vis spectrophotometry. The DLC and DLE of PPT conjugate were 21.0 wt% and 74.8%, respectively. Furthermore, the conformation of PLG-*g*-mPEG and PLG-*g*-mPEG-PPT in PB at pH 7.4 was measured by circular dichroism spectroscopy. PLG-*g*-mPEG predominantly adopted a random-coil conformation indicated by a positive maximum at 217 nm and a minimum at 201 nm in Fig. S1. The CD curve exhibited a positive maximum at 220 nm and a minimum at 209 nm, indicating that the PLG-*g*-mPEG-PPT also adopted a random-coil conformation. These should be attributed to the fact that most of the carboxyl groups on the side chain remained at an ionized status at pH 7.4. According to a report of Cheng's group [48], poly glutamic acid transform to the sodium salt form under physiological pH and the repulsion between charges is very strong. Because of the strong inter-charge force, both PLG-*g*-mPEG and PLG-*g*-mPEG-PPT kept a random-coil conformation.

3.2. Self-assembly of PLG-g-mPEG-PPT conjugate

After bonding of hydrophobic PPT, amphiphilic PLG-*g*-mPEG-PPT can self-assemble to micelles in aqueous solution. Because of the hydrophilicity of PEG segments, PLG-*g*-mPEG-PPT can be directly dissolved in water to obtain the micelles (Scheme 1B). The hydrodynamic sizes of the micelles were determined by DLS measurements. As shown in Fig. 2A, the hydrodynamic radius (R_h) of the PLG-*g*-mPEG-PPT micelles was 50.0 ± 15.1 nm, suggesting that PLG-*g*-mPEG-PPT could self-assemble into nanoscale particle in aqueous phase to maintain the balance between the hydrophilic moieties and hydrophobic ones. The size of the PLG-*g*-mPEG-PPT micelles will also bring advantages for solid tumor

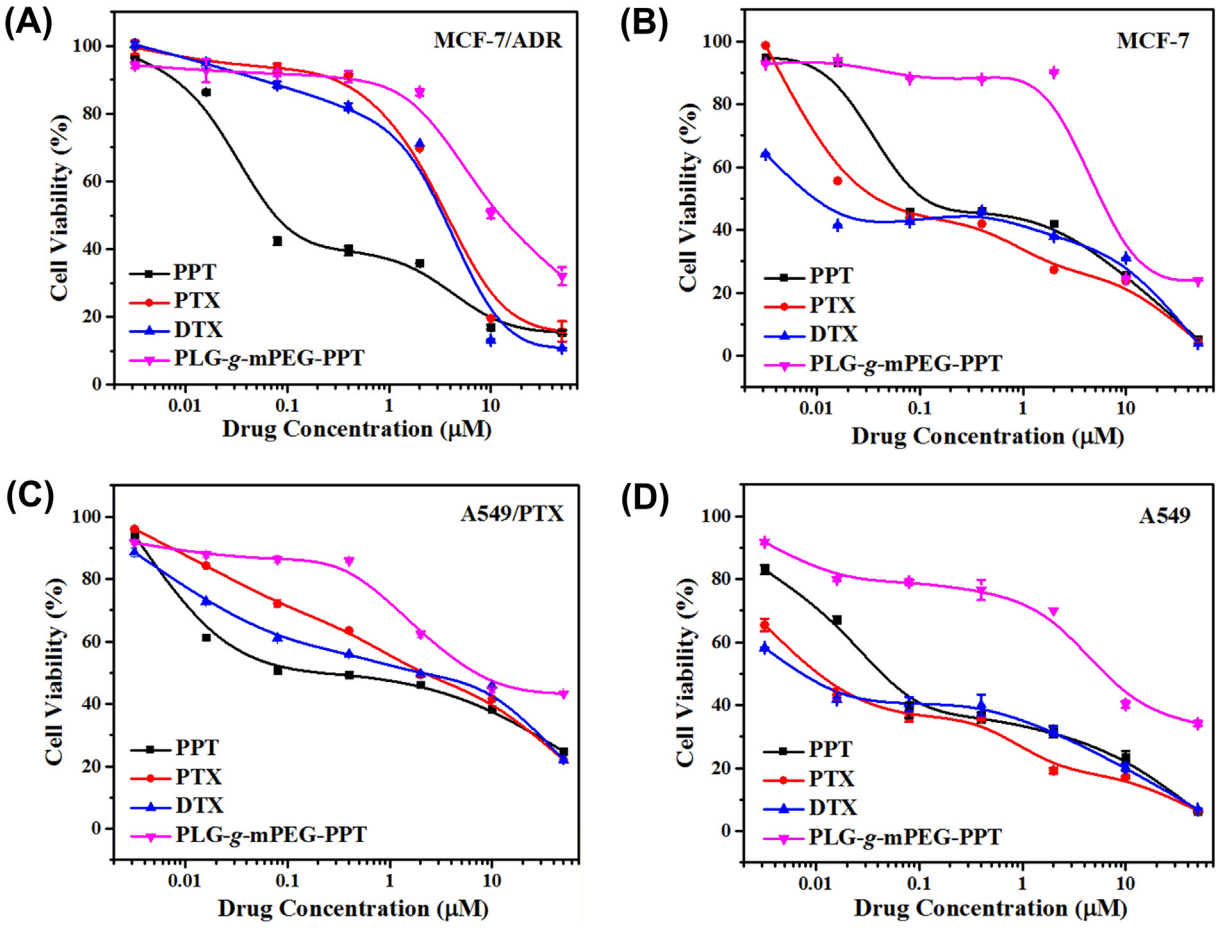

Fig. 6. *In vitro* cytotoxicity studies of PPT, PTX, DTX and PLG-*g*-mPEG-PPT on different cells for 72 h by MTT assay. (n = 3).

Table 1
The IC_{50} values and resistance index (RI) of PPT, PTX, DTX and PLG-*g*-mPEG-PPT on different cell lines for 72 h (unit of IC_{50} value: μM).

	MCF-7/ADR	MCF-7	RI	A549/PTX	A549	RI
PPT	0.12	0.12	1.00	0.31	0.03	10.33
PTX	4.89	0.04	122.30	1.23	0.01	123.00
DTX	3.74	0.01	374.00	1.19	0.004	297.50
PLG-*g*-mPEG-PPT	12.30	5.80	2.12	6.72	6.11	1.10

targeting delivery *via* EPR effect because they are large enough to avoid filtration by the kidney (R_h > 10 nm) and small enough to decrease the capture of reticulo-endothelial system (RES) [49]. After PLG-*g*-mPEG-PPT self-assembled into micellar-type nanoparticles in the aqueous phase, the self-assembly stability and the surface charge of the micelles were determined. Pyrene was used as the fluorescence probe. The CMC value of PLG-*g*-mPEG-PPT was determined to be 2.8×10^{-2} mg mL^{-1} (Fig. 2B). The zeta potential of the micelles was measured. Owing to the pendant carboxylic acid groups of the glutamic acid units, PLG-*g*-mPEG-PPT was negative charged at the physiological environment and the zeta potential was −10.5 ± 0.3 mV in water. For drug delivery systems by intravenous administration, low or neutral charge is more suitable for *in vivo* applications. Due to the strong interactions with negatively charged serum proteins, positively charged nanoparticles are not stable during blood circulation [50,51].

3.3. In vitro drug release

The PPT release profiles of PLG-*g*-mPEG-PPT were studied in PBS at various pH values (7.4 and 5.0) with and without trypsin at 37 °C. As shown in Fig. 3, PPT kept a sustained and relatively slow release rate in PBS at both pH 7.4 and 5.0 without enzyme, <10% of PPT released even when the time extended to 72 h, demonstrating the stability of the covalent ester linker between the PPT and PLG-*g*-mPEG. On the contrary, when incubated with trypsin, the micelles showed a significant increase release trend of PPT within 5 h. After that, the PPT conjugate exhibited a stable PPT release behavior for a long period of time. At the selected 72 h time point, about 74% PPT were released from the nanoparticles at pH 5.0 and about 59% PPT were released at pH 7.4. Once the PLG-*g*-mPEG nanoparticles penetrating into the tumor tissues by EPR effect, PPT could be easily released from the nanoparticles through the enzyme hydrolysis effect. In addition, considering the excellent long circulating capability and tumor accumulation of PLG-*g*-mPEG, the sustained drug release would lead to extended tumor growth inhibition *in vivo*.

3.4. Cell uptake

To investigate the cellular internalization, FI-labeled PLG-*g*-mPEG-PPT was incubated with MCF-7/ADR cells for 1 h or 3 h at 37 °C. The cell uptake was then observed by CLSM (Fig. 4), the nuclei were stained with DAPI (blue) for subcellular observation, and the green fluorescence from FI was carried out to visualize the location of PPT conjugates after internalized by MCF-7/ADR cells. For the samples, a time dependent cellular accumulation was observed as much higher fluorescent intensity was seen at 3 h than those at 1 h. After 1 h incubation at 37 °C with FI-labeled PLG-*g*-mPEG-PPT, the green fluorescence was started to appear in the cytosol and surround the nuclei. With time extended to 3 h, enhancement green fluorescence could be distinguished. This implied that more nanoparticles entered into the cells as the culture time prolonged.

3.5. Western blot analysis

In order to examine the effects of PPT and PLG-*g*-mPEG-PPT on tumor cell P-gp expression, varied concentrations of free PPT and PLG-*g*-mPEG-PPT were incubated with MCF-7/ADR cells for 48 h.

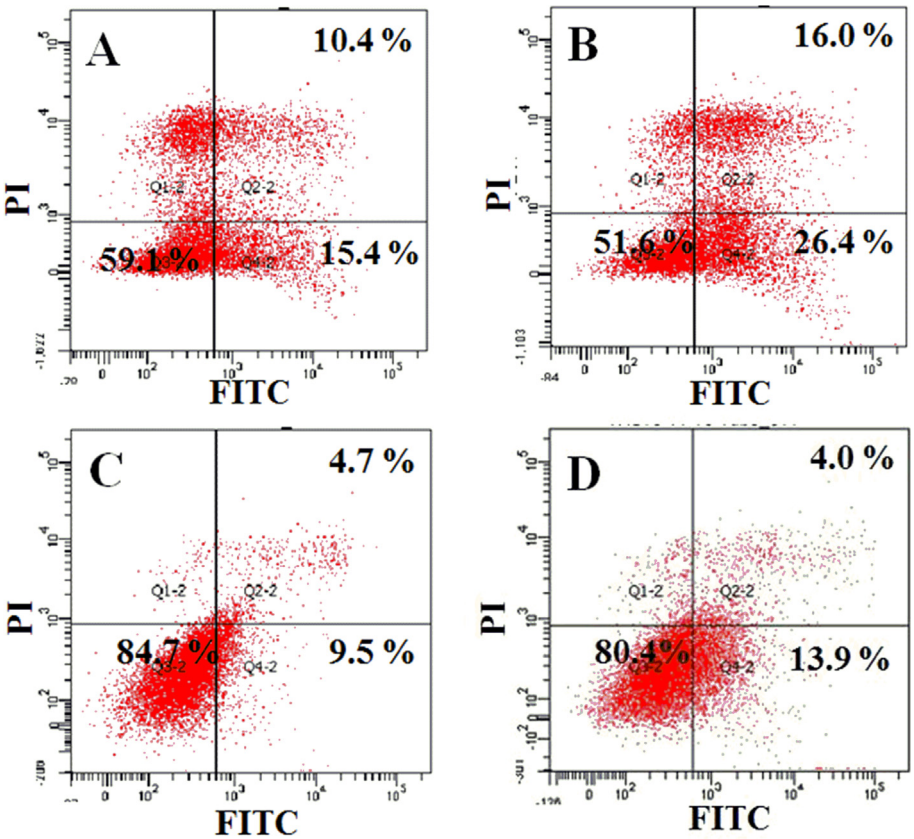

Fig. 7. Apoptotic cell populations determined by flow cytometric analysis with Annexin V-FITC and propidium iodide (PI) staining after incubating MCF-7/ADR cells for 48 h, with (A) free PPT 10 μM; (B) free PPT 20 μM; (C) PLG-*g*-mPEG-PPT 10 μM (based on PPT concentration); and (D) PLG-*g*-mPEG-PPT 20 μM (based on PPT concentration). The lower-left and upper-left quadrants in each panel indicate the populations of normal cells and necrotic cells, respectively, whereas the lower-right and upper-right quadrants in each panel indicate the populations of early and late apoptotic cells, respectively.

Total cell lysates were analysed by western blot analysis. As shown in Fig. 5A, MCF-7/ADR cells had a high P-gp expression level but it almost couldn't be detected in MCF-7 cells. Low concentration of PPT didn't affect the P-gp expression but when the concentration increased to 0.1 μM, the P-gp expression decreased obviously and exhibited dose dependence. Free PPT induced 39.4% P-gp expression down-regulation at the concentration of 2.5 μM (Fig. 5B). Similarly, PLG-*g*-mPEG-PPT induced 30.1% and 61.3% P-gp expression down-regulation at the concentration of 12.5 μM and 62.5 μM on PPT equivalent, respectively (Fig. 5D). These indicated that PLG-*g*-mPEG-PPT had as effective capacity of inhibiting P-gp expression as free PPT.

3.6. In vitro cytotoxicity and apoptotic studies

To further compare the ability of PPT and PLG-*g*-mPEG-PPT in killing drug-resistant cells with common cancer cells, the *in vivo* cytotoxicity of free PPT and PLG-*g*-mPEG-PPT were evaluated against two types of normal tumor cell lines and corresponding resistant cell lines for 72 h by MTT assay. Meanwhile, PTX and DTX, two widely used chemotherapeutic drugs, were used as the control. The resistance index (RI) was denoted as IC_{50} of resistant cell/IC_{50} of sensitive cell [36]. The MTT results were shown in Fig. 6 and Table 1. For the RI values of different cell lines showed in Table 1, the RI (72 h) of PTX and DTX against MCF-7/ADR (MCF-7) cells were about 122.3 and 374.0, respectively. The RI (72 h) of PTX and DTX against A549/PTX (A549) cells were about 123.0 and 297.5 respectively, demonstrating the disability of common chemotherapeutic drugs in the treatment of MDR cancer cells. In contrast, the RIs of free PPT against these two cell lines were 1.0 (MCF-7 and MCF-7/ADR couple) and 10.3 (A549 and A549/PTX couple), respectively. The RIs of PLG-*g*-mPEG-PPT against the two cell lines were 2.12 (equaled to 1/57.7 of PTX and 1/176.4 of DTX on MCF-7 and MCF-7/ADR couple) and 1.10 (equaled to 1/111.8 of PTX and 1/270.5 of DTX on A549 and A549/PTX couple), respectively. These were much lower than those of PTX and DTX, suggesting that free PPT and PLG-*g*-mPEG-PPT had enormous advantages in inhibiting the P-gp overexpressed MDR cancer cell lines *in vitro*.

Further, the apoptosis of MCF-7/ADR cells treated with free PPT and PLG-*g*-mPEG-PPT at different concentration was evaluated by flow cytometry. Cells were double stained for viability (negative for propidium iodide) and apoptosis (positive for Annexin V-

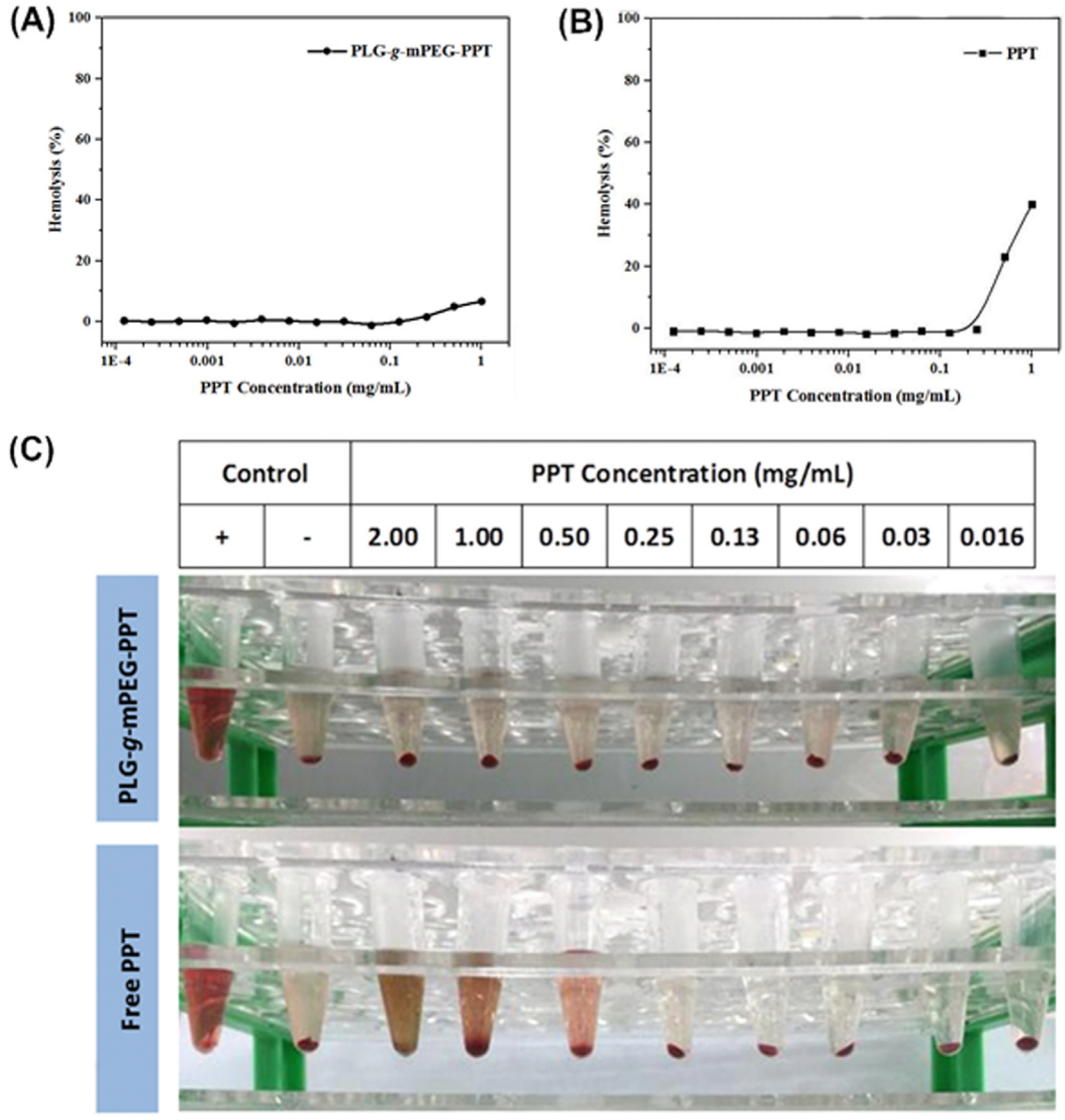

Fig. 8. Hemolytic activities of (A) PLG-*g*-mPEG-PPT, (B) Free PPT on rabbit red blood cells and (C) Photographs of hemolysis of RBCs after the treatment with PLG-*g*-mPEG-PPT and free PPT. The red hemoglobin in the supernatant indicates the damage to RBCs. Double distilled water and PBS are used as positive (+) and negative (−) controls, respectively. (For interpretation of the references to colour in this figure legend, the reader is referred to the web version of this article.)

FITC). Incubated with the cells at a concentration of 10 μM PPT-equivalent for 48 h, free PPT and the PLG-*g*-mPEG-PPT resulted in 15.4% and 9.5% early apoptotic cells, respectively (Fig. 7). A higher ratio of early apoptotic cells (26.4% and 13.9%) were observed for both the free PPT and PLG-*g*-mPEG-PPT at 20 μM PPT equivalent. Similarly to the MTT assay results, the decreased apoptotic activity of PLG-*g*-mPEG-PPT compared with free PPT is probably due to the relatively low level of cell uptake through endocytosis during the endocytosis process.

3.7. Safety evaluation of the drug conjugate

Stabile blood compatibility of the drug-loaded micelle is crucial, because it will be finally injected intravenously into blood vessels. A hemolysis assay was carried out based on the previous report [52,53]. As shown in Fig. 8A, PLG-*g*-mPEG-PPT showed slight hemolysis toxicity (<10%) to RBCs at the concentration of 1.0 mg mL^{-1} but for free PPT it was about 50% hemolysis (Fig. 8B), demonstrating the excellent blood compatibility of PPT conjugate. The photographs of the RBC samples also showed that PLG-*g*-mPEG-PPT could significantly decrease the hemolysis of the RBCs compared to free PPT (Fig. 8C). The low hemolytic activity should be originated from the PEG shell serving as a protective layer, and the negatively charged surface of the PLG-*g*-mPEG-PPT micelle [54].

The MTD was assessed in tumor-free Kunming mice. The mice were administered intravenously with different doses of free PPT or PPT conjugates, followed by daily body weight measurement and observation of toxic death. As shown in Fig. 9A, the MTD of free PPT was 15 mg kg^{-1}, basically consistent with the previous literature report [36]. In contrast, the MTD of PLG-*g*-mPEG-PPT was 200 mg kg^{-1} (PPT-equivalent), increasing about 13.3 folds than that of free PPT. Except for the death group, no weight loss was observed in all groups (Fig. 9B, D). As far as we know, once small molecule PPT was administrated, it could exert toxicity to the body immediately and induce death of mice soon after 1 or 2 days. But for PLG-*g*-mPEG-PPT, it possessed a sustained PPT release progress and the drug was persistent to be effective, so it needed a long period of time to produce side effect. In summary, the high MTD for PPT conjugate may be attributed to the slow release kinetics of PPT under physiological conditions (Fig. 3) and the remarkable biocompatibility and safety of the PLG-*g*-mPEG vehicle.

3.8. In vivo antitumor efficacy

To evaluate the antitumor activity of PLG-*g*-mPEG-PPT, efficacy studies were performed in mice bearing MCF-7/ADR xenografts. After the tumor volume reached about 60 mm^3, mice were treated with free PPT or PLG-*g*-mPEG-PPT for only one time at 15 and 200 mg kg^{-1} (PPT equivalents at the MTD respectively) *via* the tail vein. PBS was used as a control. The tumor volumes and the body weights were measured. As shown in Fig. 10A, the tumor volumes in the control group (PBS) increased progressively rapidly to over 830.0 mm^3 in 30 days. For the free PPT group, the tumors were

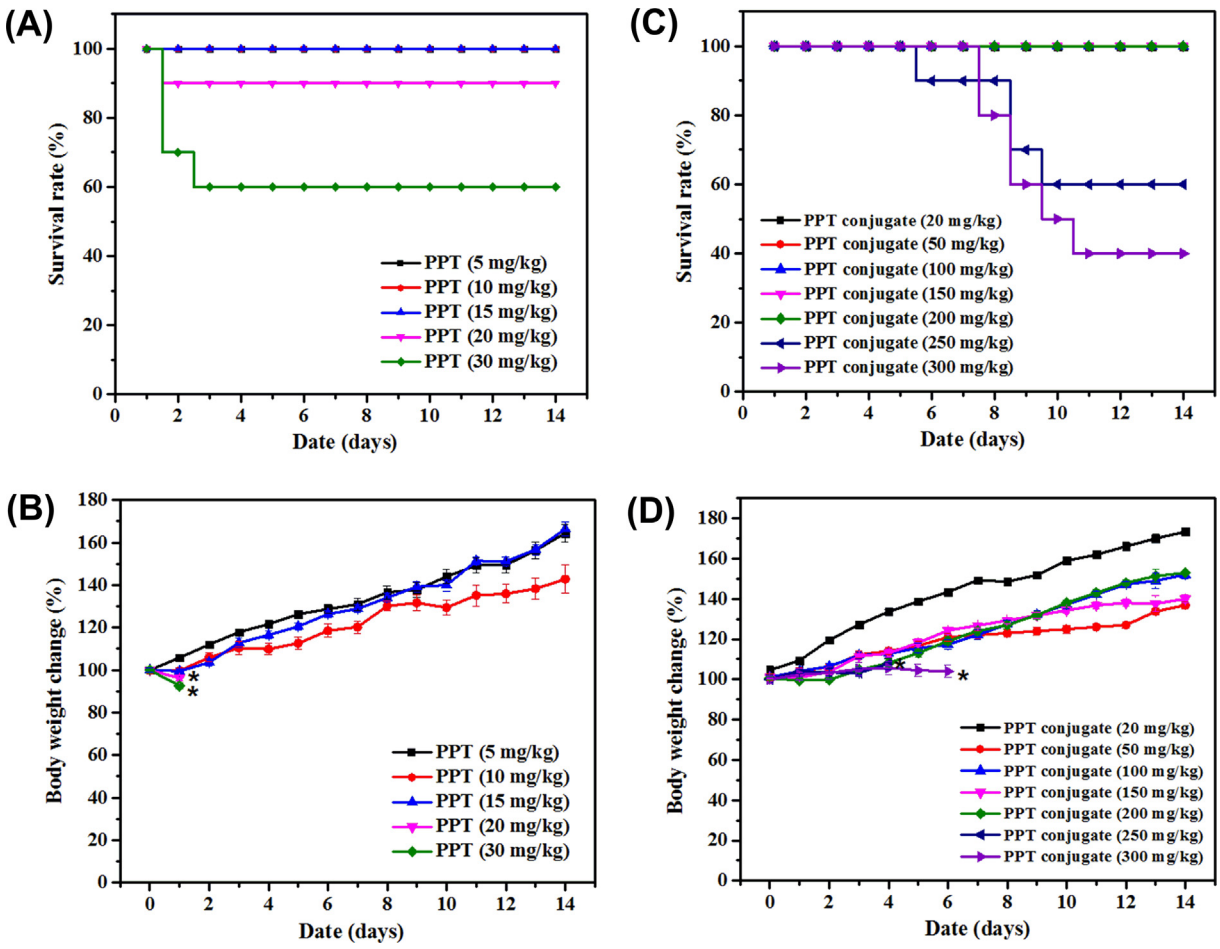

Fig. 9. MTD studies for free PPT and PLG-*g*-mPEG-PPT (PPT conjugate) on survival rate and body weight change in tumor-free Kunming mice: (A, B) survival rate and body weight change for free PPT; (C, D) survival rate and body weight change for PLG-*g*-mPEG-PPT.

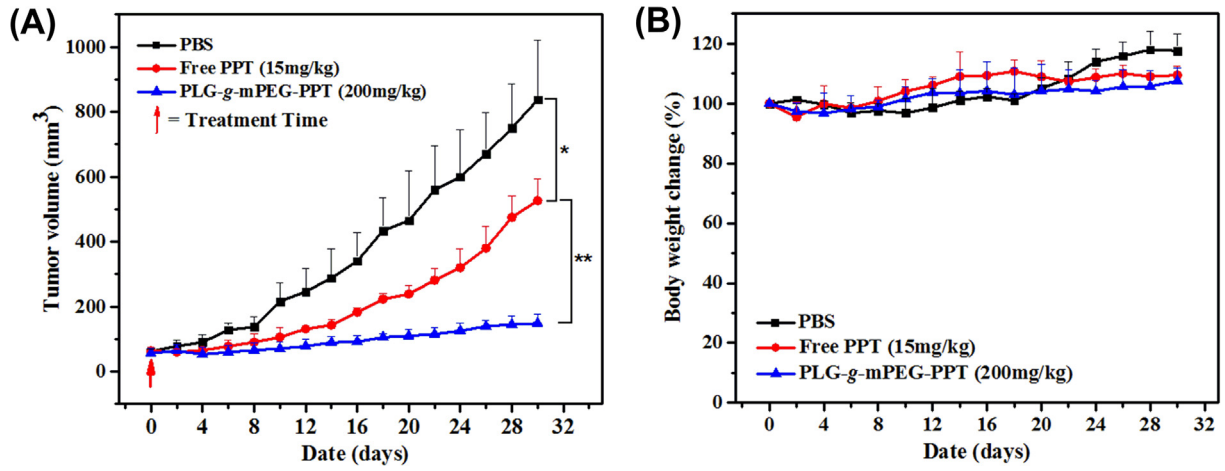

Fig. 10. Effect of PPT and PLG-*g*-mPEG-PPT on anti-tumor efficacy in term of (A) tumor volume, (B) body weight change in MCF-7/ADR xenograft-bearing nude mice. The data are shown as mean ± SD (n = 4), $^{*}p < 0.01$, $^{**}p < 0.001$.

temporarily controlled in the initial 4 days, but afterwards the tumors began to grow quickly. The tumor volume increased to 526.7 ± 64.7 mm^3 at the end of the free PPT treatment, showed a negligible reduction in tumor volume (TSR = 37.1%). In contrast, PLG-*g*-mPEG-PPT demonstrated persistent tumor growth inhibitory effect. The tumor volume increased to only 146 ± 27.5 mm^3 at the end of the treatment, showed a tumor suppression rate (TSR) of 82.5%. For all groups, no animals' weight loss and visible adverse effects were observed during the study (Fig. 10B). As far as we know, there is a great difference between environment of cell culture and the tumor microenvironment. Nanoparticles can accumulate at the tumor site through enhanced permeability and retention (EPR) effect and PPT can continuous release from the NPs under the action of enzymes in the tumor microenvironment. In addition, the MTD of PLG-*g*-mPEG-PPT increased greatly (13.3 folds) as compared to that of free PPT, therefore, the *in vivo* dose of PLG-*g*-mPEG-PPT was much higher than free PPT with minimal toxicity. All above results demonstrated that the PLG-*g*-mPEG-PPT possessed enhanced *in vivo* antitumor efficacy by significantly improving the MTD with the good performance of PLG-*g*-mPEG vehicle and combining the excellent killing effect of PPT to MDR cancer cells, indicating that the PLG-*g*-mPEG-PPT is promising in MDR cancer therapy.

4. Conclusions

In summary, a polypeptide conjugate for the treatment of multiple drug resistant breast cancer was developed by conjugating podophyllotoxin to a water soluble PLG-*g*-mPEG polymer. *In vitro* studies demonstrated significant cell proliferation inhibition effect and hundredfold reduction on RI values of PLG-*g*-mPEG-PPT against MCF-7/ADR and A549/PTX cell lines. PLG-*g*-mPEG-PPT could also reduce the P-gp expression level of MCF-7/ADR cells, which was advantageous to combat the MDR efficiently just by a single agent. PLG-*g*-mPEG-PPT showed improved safety profiles with decreased hemolytic activity and a significant improvement in MTD (13.3 folds to free PPT). Through the *in vivo* studies, we confirmed that the PLG-*g*-mPEG-PPT remarkably enhanced the antitumor efficacy against MCF-7/ADR xenograft tumors with a TSR of 82.5%, which was much higher than of PPT (37.1%), displayed a vigorous tumor inhibition effect on MDR human breast tumor xenograft model. This investigation provides a simple and effective nanomedicine for overcome MDR in cancer therapy.

Acknowledgments

This research was financially supported by National Natural Science Foundation of China (Projects 51390484, 51473141, 51673189, 51273169, 51503202, 51473029 and 51673185), the Program of Scientific Development of Jilin Province (No. 20170101100JC) and the Chinese Academy of Sciences Youth Innovation Promotion Association.

References

[1] E. Blanco, A. Hsiao, A.P. Mann, M.G. Landry, F. Meric-Bernstam, M. Ferrari, Nanomedicine in cancer therapy: innovative trends and prospects, Cancer Sci. 102 (7) (2011) 1247–1252.
[2] A.B. Parikh, P. Kozuch, N. Rohs, D.J. Becker, B.P. Levy, Metformin as a repurposed therapy in advanced non-small cell lung cancer (NSCLC): results of a phase II trial, Invest. New Drugs 35 (6) (2017) 813–819.
[3] E. Perez-Herrero, A. Fernandez-Medarde, Advanced targeted therapies in cancer: Drug nanocarriers, the future of chemotherapy, Eur. J. Pharm. Biopharm. 93 (2015) 52–79.
[4] H. Maeda, Toward a full understanding of the EPR effect in primary and metastatic tumors as well as issues related to its heterogeneity, Adv. Drug Del. Rev. 91 (2015) 3–6.
[5] J. Shi, P.W. Kantoff, R. Wooster, O.C. Farokhzad, Cancer nanomedicine: progress, challenges and opportunities, Nat. Rev. Cancer 17 (1) (2017) 20–37.
[6] H. Zhou, H. Sun, S. Lv, D. Zhang, X. Zhang, Z. Tang, X. Chen, Legumain-cleavable 4-arm poly(ethylene glycol)-doxorubicin conjugate for tumor specific delivery and release, Acta Biomater. 54 (2017) 227–238.
[7] S. Lv, Z. Tang, W. Song, D. Zhang, M. Li, H. Liu, J. Cheng, W. Zhong, X. Chen, Inhibiting solid tumor growth in vivo by non-tumor-penetrating nanomedicine, Small 13 (12) (2017).
[8] S. Lv, Y. Wu, J. Dang, Z. Tang, Z. Song, S. Ma, X. Wang, X. Chen, J. Cheng, L. Yin, Investigation on the controlled synthesis and post-modification of poly-(N-2-hydroxyethyl)aspartamide-based polymers, Polym. Chem. 8 (12) (2017) 1872–1877.
[9] T. Ojha, V. Pathak, Y. Shi, W.E. Hennink, C.T.W. Moonen, G. Storm, F. Kiessling, T. Lammers, Pharmacological and physical vessel modulation strategies to improve EPR-mediated drug targeting to tumors, Adv. Drug Del. Rev. 119 (2017) 44–60.
[10] K.K. Upadhyay, J.F. Le Meins, A. Misra, P. Voisin, V. Bouchaud, E. Ibarboure, C. Schatz, S. Lecommandoux, Biomimetic doxorubicin loaded polymersomes from hyaluronan-block-poly(gamma-benzyl glutamate) copolymers, Biomacromolecules 10 (10) (2009) 2802–2808.
[11] C. Bonduelle, H. Oliveira, C. Gauche, J. Huang, A. Heise, S. Lecommandoux, Multivalent effect of glycopolypeptide based nanoparticles for galectin binding, Chem. Commun. 52 (75) (2016) 11251–11254.
[12] M. Nguyen, J.-L. Stigliani, G. Pratviel, C. Bonduelle, Nucleopolypeptides with DNA-triggered alpha helix-to-beta sheet transition, Chem. Commun. 53 (54) (2017) 7501–7504.
[13] Z. Song, Z. Han, S. Lv, C. Chen, L. Chen, L. Yin, J. Cheng, Synthetic polypeptides: from polymer design to supramolecular assembly and biomedical application, Chem. Soc. Rev. 46 (21) (2017) 6570–6599.
[14] H. Yu, Z. Tang, D. Zhang, W. Song, Y. Zhang, Y. Yang, Z. Ahmad, X. Chen, Pharmacokinetics, biodistribution and in vivo efficacy of cisplatin loaded poly

(L-glutamic acid)-g-methoxy poly (ethylene glycol) complex nanoparticles for tumor therapy, J. Controlled Release 205 (2015) 89–97.
[15] M. Dean, T. Fojo, S. Bates, Tumour stem cells and drug resistance, Nat. Rev. Cancer 5 (4) (2005) 275–284.
[16] G. Szakacs, J.K. Paterson, J.A. Ludwig, C. Booth-Genthe, M.M. Gottesman, Targeting multidrug resistance in cancer, Nat. Rev. Drug Discov. 5 (3) (2006) 219–234.
[17] P. Joshi, R.A. Vishwakarma, S.B. Bharate, Natural alkaloids as P-gp inhibitors for multidrug resistance reversal in cancer, Eur. J. Med. Chem. 138 (2017) 273–292.
[18] L.-M. Mu, R.-J. Ju, R. Liu, Y.-Z. Bu, J.-Y. Zhang, X.-Q. Li, F. Zeng, W.-L. Lu, Dual-functional drug liposomes in treatment of resistant cancers, Adv. Drug Del. Rev. 115 (2017) 46–56.
[19] Z. Chen, T. Shi, L. Zhang, P. Zhu, M. Deng, C. Huang, T. Hu, L. Jiang, J. Li, Mammalian drug efflux transporters of the ATP binding cassette (ABC) family in multidrug resistance: a review of the past decade, Cancer Lett. 370 (1) (2016) 153–164.
[20] F. Ren, J. Shen, H. Shi, F.J. Hornicek, Q. Kan, Z. Duan, Novel mechanisms and approaches to overcome multidrug resistance in the treatment of ovarian cancer, Biochim. Biophys. Acta 1866 (2) (2016) 266–275.
[21] Y. Chen, O. Tezcan, D. Li, N. Beztsinna, B. Lou, T. Etrych, K. Ulbrich, J.M. Metselaar, T. Lammers, W.E. Hennink, Overcoming multidrug resistance using folate receptor-targeted and pH-responsive polymeric nanogels containing covalently entrapped doxorubicin, Nanoscale 9 (29) (2017) 10404–10419.
[22] S. Kunjachan, B. Rychlik, G. Storm, F. Kiessling, T. Lammers, Multidrug resistance: Physiological principles and nanomedical solutions, Adv. Drug Del. Rev. 65 (13–14) (2013) 1852–1865.
[23] H.M. Coley, Mechanisms and strategies to overcome chemotherapy resistance in metastatic breast cancer, Cancer Treat. Rev. 34 (4) (2008) 378–390.
[24] Y. Zhao, Y. Zhou, D. Wang, Y. Gao, J. Li, S. Ma, L. Zhao, C. Zhang, Y. Liu, X. Li, pH-responsive polymeric micelles based on poly(2-ethyl-2-oxazoline)-poly(D,L-lactide) for tumor-targeting and controlled delivery of doxorubicin and P-glycoprotein inhibitor, Acta Biomater. 17 (2015) 182–192.
[25] R.J. Kathawala, P. Gupta, C.R. Ashby Jr., Z.-S. Chen, The modulation of ABC transporter-mediated multidrug resistance in cancer: a review of the past decade, Drug Resist. Update. 18 (2015) 1–17.
[26] C. Avendano, J.C. Menendez, Inhibitors of multidrug resistance to antitumor agents (MDR), Curr. Med. Chem. 9 (2) (2002) 159–193.
[27] G.C. Tomskey, G.W. Vickery, P.L. Getzoff, The successful treatment of granuloma inguinale, with special reference to the use of podophyllin, J. Urol. 48 (4) (1942) 401–406.
[28] A. Giri, M.L. Narasu, Production of podophyllotoxin from *Podophyllum hexandrum*: a potential natural product for clinically useful anticancer drugs, Cytotechnology 34 (1–2) (2000) 17–26.
[29] X. Yu, Z. Che, H. Xu, Recent advances in the chemistry and biology of podophyllotoxins, Chem. Eur. J. 23 (19) (2017) 4467–4526.
[30] L. Zhang, F. Chen, J. Wang, Y. Chen, Z. Zhang, Y. Lin, X. Zhu, Novel isatin derivatives of podophyllotoxin: synthesis and cytotoxic evaluation against human leukaemia cancer cells as potent anti-MDR agents, Rsc Adv. 5 (118) (2015) 97816–97823.
[31] H.M. Abdallah, A.M. Al-Abd, R.S. El-Dine, A.M. El-Halawany, P-glycoprotein inhibitors of natural origin as potential tumor chemo-sensitizers: a review, J. Adv. Res. 6 (1) (2015) 45–62.
[32] S. Zhu, H. Zhen, Y. Li, P. Wang, X. Huang, P. Shi, PEGylated graphene oxide as a nanocarrier for podophyllotoxin, J. Nanopart. Res. 16 (8) (2014).
[33] X. Huang, X. Huang, X.-H. Jiang, F.-Q. Hu, Y.-Z. Du, Q.-F. Zhu, C.-S. Jin, In vitro antitumour activity of stearic acid-g-chitosan oligosaccharide polymeric micelles loading podophyllotoxin, J. Microencaps. 29 (1) (2012) 1–8.
[34] L. Fan, H. Wu, H. Zhang, F. Li, T.-H. Yang, pH-sensitive podophyllotoxin carrier for cancer cells specific delivery, Polym. Compos. 31 (1) (2010) 51–59.
[35] H.B. Chen, X.L. Chang, D.R. Du, W. Liu, J. Liu, T. Weng, Y.J. Yang, H.B. Xu, X.L. Yang, Podophyllotoxin-loaded solid lipid nanoparticles for epidermal targeting, J. Controlled Release 110 (2) (2006) 296–306.
[36] A. Roy, M.J. Ernsting, E. Undzys, S.-D. Li, A highly tumor-targeted nanoparticle of podophyllotoxin penetrated tumor core and regressed multidrug resistant tumors, Biomaterials 52 (2015) 335–346.
[37] A. Roy, Y. Zhao, Y. Yang, A. Szeitz, T. Klassen, S.-D. Li, Selective targeting and therapy of metastatic and multidrug resistant tumors using a long circulating podophyllotoxin nanoparticle, Biomaterials 137 (2017) 11–22.
[38] W. Song, Z. Tang, D. Zhang, Y. Zhang, H. Yu, M. Li, S. Lv, H. Sun, M. Deng, X. Chen, Anti-tumor efficacy of c(RGDfK)-decorated polypeptide-based micelles co-loaded with docetaxel and cisplatin, Biomaterials 35 (9) (2014) 3005–3014.
[39] W. Song, Z. Tang, M. Li, S. Lv, H. Sun, M. Deng, H. Liu, X. Chen, Polypeptide-based combination of paclitaxel and cisplatin for enhanced chemotherapy efficacy and reduced side-effects, Acta Biomater. 10 (3) (2014) 1392–1402.
[40] S. Lv, M. Li, Z. Tang, W. Song, H. Sun, H. Liu, X. Chen, Doxorubicin-loaded amphiphilic polypeptide-based nanoparticles as an efficient drug delivery system for cancer therapy, Acta Biomater. 9 (12) (2013) 9330–9342.
[41] F. Shi, J. Ding, C. Xiao, X. Zhuang, C. He, L. Chen, X. Chen, Intracellular microenvironment responsive PEGylated polypeptide nanogels with ionizable cores for efficient doxorubicin loading and triggered release, J. Mater. Chem. 22 (28) (2012) 14168–14179.
[42] W. Song, Z. Tang, D. Zhang, M. Li, J. Gu, X. Chen, A cooperative polymeric platform for tumor-targeted drug delivery, Chem. Sci. 7 (1) (2016) 728–736.
[43] T. Liu, D. Zhang, W. Song, Z. Tang, J. Zhu, Z. Ma, X. Wang, X. Chen, T. Tong, A poly(L-glutamic acid)-combretastatin A4 conjugate for solid tumor therapy: markedly improved therapeutic efficiency through its low tissue penetration in solid tumor, Acta Biomater. 53 (2017) 179–189.
[44] H. Yu, Z. Tang, M. Li, W. Song, D. Zhang, Y. Zhang, Y. Yang, H. Sun, M. Deng, X. Chen, Cisplatin loaded poly(L-glutamic acid)-g-methoxy poly(ethylene glycol) complex nanoparticles for potential cancer therapy: preparation, in vitro and in vivo evaluation, J. Biomed. Nanotechnol. 12 (1) (2016) 69–78.
[45] W. Song, Z. Tang, N. Shen, H. Yu, Y. Jia, D. Zhang, J. Jiang, C. He, H. Tian, X. Chen, Combining disulfiram and poly(L-glutamic acid)-cisplatin conjugates for combating cisplatin resistance, J. Control. Release 231 (2016) 94–102.
[46] H.Y. Yifei Li, Hai Sun, Jianguo Liu, Zhaohui Tang, Dan Wang, Yu Lianyou, Xuesi Chen, Cisplatin-loaded poly(L-glutamic acid)-g-methoxy poly(ethylene glycol) nanoparticles as a potential chemotherapeutic agent against osteosarcoma, Chin. J. Polym. Sci. 33 (5) (2015) 763–771.
[47] K. Kurihara, T. Abe, N. Higashi, M. Niwa, Steric forces between brush layers of poly (L-glutamic acid) and their dependence on secondary structures as determined by FT-IR spectroscopy, Colloids Surf. Physicochem. Eng. Aspects 103 (3) (1995) 265–272.
[48] H. Lu, J. Wang, Y. Bai, J.W. Lang, S. Liu, Y. Lin, J. Cheng, Ionic polypeptides with unusual helical stability, Nat. Commun. 2 (2011) 206.
[49] X. Duan, Y. Li, Physicochemical characteristics of nanoparticles affect circulation biodistribution, cellular internalization, and trafficking, Small 9 (9–10) (2013) 1521–1532.
[50] J.A. Barreto, W. O'Malley, M. Kubeil, B. Graham, H. Stephan, L. Spiccia, Nanomaterials: applications in cancer imaging and therapy, Adv. Mater. 23 (12) (2011) H18–H40.
[51] V.P. Chauhan, R.K. Jain, Strategies for advancing cancer nanomedicine, Nat. Mater. 12 (11) (2013) 958–962.
[52] W. Song, M. Li, Z. Tang, Q. Li, Y. Yang, H. Liu, T. Duan, H. Hong, X. Chen, Methoxypoly(ethylene glycol)-block-poly(L-glutamic acid)-loaded cisplatin and a combination with irgd for the treatment of non-small-cell lung cancers, Macromol. Biosci. 12 (11) (2012) 1514–1523.
[53] L. Zhao, J. Ding, C. Xiao, P. He, Z. Tang, X. Pang, X. Zhuang, X. Chen, Glucose-sensitive polypeptide micelles for self-regulated insulin release at physiological pH, J. Mater. Chem. 22 (24) (2012) 12319–12328.
[54] Q. Xiao, W. Bu, Q. Ren, S. Zhang, H. Xing, F. Chen, M. Li, X. Zheng, Y. Huab, L. Zhou, W. Peng, H. Qu, Z. Wang, K. Zhao, J. Shi, Radiopaque fluorescence-transparent TaOx decorated upconversion nanophosphors for in vivo CT/MR/UCL trimodal imaging, Biomaterials 33 (30) (2012) 7530–7539.